Valence band changes in Sb2-xInxTe3 and Sb2Te3-ySey by transprot and Shubnikov-de Haas effect measurements

Kulbachinskii, V.A.; Dashevski, Z.M.; Inoue, M.; Sasaki, M.; Negishi, H.; Gao, W.X.; Lostak, P.; Horak, J.; de Visser, A.

DOI
10.1103/PhysRevB.52.10915

Publication date
1995

Published in
Physical Review. B, Condensed Matter

Valence-band changes in $Sb_{2-x}In_xTe_3$ and $Sb_2Te_{3-y}Se_y$ by transport and Shubnikov–de Haas effect measurements

V. A. Kulbachinskii and Z. M. Dashevskii
Low Temperature Physics Department, Physics Faculty, Moscow State University, 119899 Moscow, Russia

M. Inoue, M. Sasaki, H. Negishi, and W. X. Gao
Department of Materials Science, Faculty of Science, Hiroshima University, Higashi-Hiroshima 739, Japan

P. Lostak and J. Horak
University of Pardubice, 532 10 Pardubice, Czech Republic

A. de Visser
Van der Waals–Zeeman Laboratory, Amsterdam University, 1018 XE Amsterdam, The Netherlands
(Received 16 May 1995)

Measurements of galvanomagnetic effects in the temperature range 4.2–300 K and photoinduced "transient thermoelectric effect" (TTE) along the C_2 axis at 300 K have been made for two types of solid solutions of semiconductors $Sb_{2-x}In_xTe_3$ ($0 \le x \le 0.4$) and $Sb_2Te_{3-y}Se_y$ ($0 \le y \le 1.8$). By incorporating In atoms into the Sb_2Te_3 lattices, Hall coefficients, Hall mobilities, and the frequencies of Shubnikov–de Haas (SdH) oscillations are varied systematically. For $Sb_2Te_{3-y}Se_y$, the Hall mobility is decreased with y up to $y=0.7$ and then increased appreciably in the range $0.7 < y < 1.8$, and a frequency component of SdH oscillations is observed for $y \ge 0.25$. The observed TTE voltages decay exponentially with time, showing a multirelaxation process with characteristic relaxation times τ_i ($i=1,2,\ldots$) for thermal diffusions of photoinduced conduction carriers, whose analyses give valuable information about carrier mobilities and effective masses. In the host material Sb_2Te_3, four relaxation times τ_i ($i=1$–4) are found, which are attributable to holes in the anisotropic upper and lower valence bands with effective-mass anisotropies of about 3. In addition, we have found two kinds of extra relaxation times τ_i ($i=5$ and 6) for $y > 0.6$ in $Sb_2Te_{3-y}Se_y$, confirming the existence of a valence band, whose anisotropy in the effective mass along the C_2 direction is evaluated to be of the order of 2–2.5. Based on these experimental data we have proposed the most probable band model for these solid solutions.

I. INTRODUCTION

Antimony telluride Sb_2Te_3 belongs to a layered compound with the same tetradymite structure as Bi_2Te_3, in which a weak bond between Sb and Te layers exists. It usually involves antistructural defects (the occurrence of Sb atoms occupying Te lattice positions). Due to such native defects, Sb_2Te_3 always shows a p-type conductivity with the hole concentration up to 10^{20} cm^{-3}. The upper valence band (UVB) of Sb_2Te_3 consists of six ellipsoids tilted to the basal plane[1,2] (Drabble-Wolf model)[3] and the lower valence band (LVB), which is known to be a multivalley, but the anisotropy of this valley is unknown; there is a publication about a single valley model for LVB.[4] The value of the tilt angle θ is not known exactly, but $\theta \cong 50°$ according to the extrapolation to $x=1$ in $(Bi_{1-x}Sb_x)_2Te_3$.[2] The energy separation between the tops of the UVB and LVB is reported to be 150 meV,[1] but this value seems to be quite large; it may be of the order of 20–30 meV, because that for $(Bi_{1-x}Sb_x)_2Te_3$ ($0 < x < 1$) is about 30 meV.[2] Furthermore, Sb_2Te_3 based solid solutions have been studied;[5–9] for example, the plasma frequency at room temperature,[5] the lattice parameter and conductivity at room temperature[6] are known for $Sb_{2-x}In_xTe_3$. According to optical studies at room temperature, the energy gap between UVB and lower electron band is increased by substituting In for $Sb_{2-x}In_xTe_3$ mixed crystals.[7,8]

For further understanding of Sb_2Te_3 based solid solutions, in the present work, we have carried out measurements of dc transport quantities in the temperature range 4.2–300 K, Shubnikov–de Haas (SdH) effect at 4.2 K in magnetic fields up to 35 T, and of pulsed laser induced "transient thermoelectric effect" (TTE) for $Sb_{2-x}In_xTe_3$ ($0 \le x \le 0.4$) and $Sb_2Te_{3-y}Se_y$ ($0 \le y \le 1.8$) single crystals along the C_2 axis at 300 K. The TTE method is a dynamic technique for understanding transport properties of multicarrier systems of electrons and holes, as evidenced for silicon,[10] GaAs,[11] quasi-two-dimensional charge-density-wave material η-Mo_4O_{11},[12] semimetal Bi,[13] and narrow gap semiconductor $Bi_{2-x}Sn_xTe_3$.[14] We are interested in the effect of the In or Se substitution on the electronic properties of the host Sb_2Te_3 and getting valuable information about the changing of its energy spectrum, in particular, the valence bands.

II. EXPERIMENT

$Sb_{2-x}In_xTe_3$ and $Sb_2Te_{3-y}Se_y$ single crystals were grown by a modified Bridgman method from $5N$ purity elements. The starting elements in the stoichiometric ratios were synthesized in evacuated conical silica ampoules. The crystals were easily cleaved perpendicular to the trigonal C_3 axis, i.e., along the (0001) (or in the C_1C_2) plane. The In and Se contents in the mixed crystals were determined by x-ray microprobe analyses. Samples for transport measurements were cut from cleaved single-crystal plates by a spark erosion machine (typical dimensions: $5\times1.5\times0.4$ mm^3).

For the investigation of the SdH effect, we used the experimental facilities with a pulse magnet available up to 35 T, at the University of Amsterdam. The resistivity and Hall effect were measured by a potentiometric method with the dc along the C_2 direction in magnetic fields up to 7 T applied along the C_3 axis (perpendicular to the layers), using a superconducting solenoid. The experimental setup and measuring principle of the TTE method have been described earlier.[10–14] In principle, a pulsed laser (laser power ~350 mJ) produced by a Nd:YAG laser source with the wavelength of 1060 nm (=1.17 eV) and pulse width of 8 ns was irradiated normal to one end of crystal. Photoinduced TTE voltages were detected over the wide time range 50 ns to 500 ms by a digital storage oscilloscope through a homemade preamplifier, whose output signal was fed to a computer for record and numerical analysis. TTE measurements were made only at 300 K, below which the TTE signals became too small to be detectable.

III. EXPERIMENTAL RESULTS

A. Galvanomagnetic effect and Shubnikov–de Haas effect

Figures 1(a) and 1(b) show the temperature dependence of the resistivity ρ for $Sb_{2-x}In_xTe_3$ ($x=0.02$, 0.1, 0.2, and 0.4) and $Sb_2Te_{3-y}Se_y$ ($y=0$, 1.0, 1.6, and 1.8) along the C_2 direction in logarithmic scales, respectively. For all samples, ρ decreases with decreasing temperature and then approaches a constant value at low temperatures. Residual resistivities increase with the substitution of In or Se atoms, which are due to the increased ionized or neutral impurity scatterings. In the temperature range 77–300 K, the $\rho-T$ curves for $Sb_2Te_{3-y}Se_y$ obey a power low of the form $\rho=T^n$, with the exponent $n\cong1.3$ for all samples.

The Hall coefficient R_H is positive for all samples and is almost independent of temperature in the whole temperature range 4.2–300 K and of a magnetic field up to 7 T. The values of R_H and the Hall mobilities μ_H at 4.2 K are plotted against the In or Se content for $Sb_{2-x}In_xTe_3$ and $Sb_2Te_{3-y}Se_y$ in Figs. 2(a) and 2(b), respectively. The Hall coefficient increases monotonically with increasing the concentration of In or Se, which indicates that the apparent hole concentrations decrease with x or y. On the other hand, the Hall mobility μ_H decreases drastically with increasing x for $Sb_{2-x}In_xTe_3$, while for $Sb_2Te_{3-y}Se_y$ it falls at a low Se concentration ($y\leq0.7$)

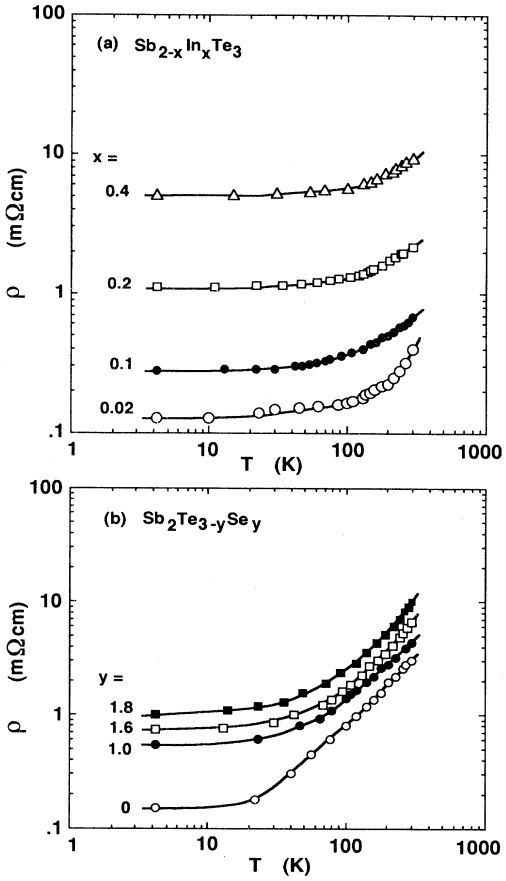

FIG. 1. Temperature dependence of the resistivity along the C_2 axis for (a) $Sb_{2-x}In_xTe_3$ ($0\leq x\leq0.4$) and (b) $Sb_2Te_{3-y}Se_y$ ($0\leq y\leq1.8$).

and then increases up to $y=1.8$ (which becomes higher than that for the host material), followed by a decrease. The drastic decrease in μ_H with x for $Sb_{2-x}In_xTe_3$ may be due to an appreciable increase of vacancies, as found for In_2Te_3 or In_2Se_3 crystals.[15,16] For the $Sb_2Te_{3-y}Se_y$ system, the increase in μ_H for $y>0.7$ is due to the predominance of a valence band with a smaller effective mass compared to those of the main UVB and LVB, as described later.

The magnetoresistance of these crystals is proportional to the square of a magnetic field B at a low magnetic fields, while it shows SdH oscillations at high fields. Figure 3 shows typical results for $Sb_{2-x}In_xTe_3$ ($x=0$, 0.02, and 0.2) at 4.2 K. In the present orientation of B parallel to the C_3 axis, we have observed a single frequency, which indicates that the extremal cross sections of the six ellipsoids of the Fermi surfaces coincide. Due to a very sharp decrease in the Hall mobility with increasing In content of $Sb_{2-x}In_xTe_3$, the oscillation amplitude falls rapidly with x; even for $x=0.2$, it was impossible to detect the SdH effect in magnetic fields up to 35 T.

Figure 4 shows similar SdH signals at 4.2 K for $Sb_2Te_{3-y}Se_3$, with Se concentrations up to $y=1.8$, where we see that a beating in the SdH oscillations appears for

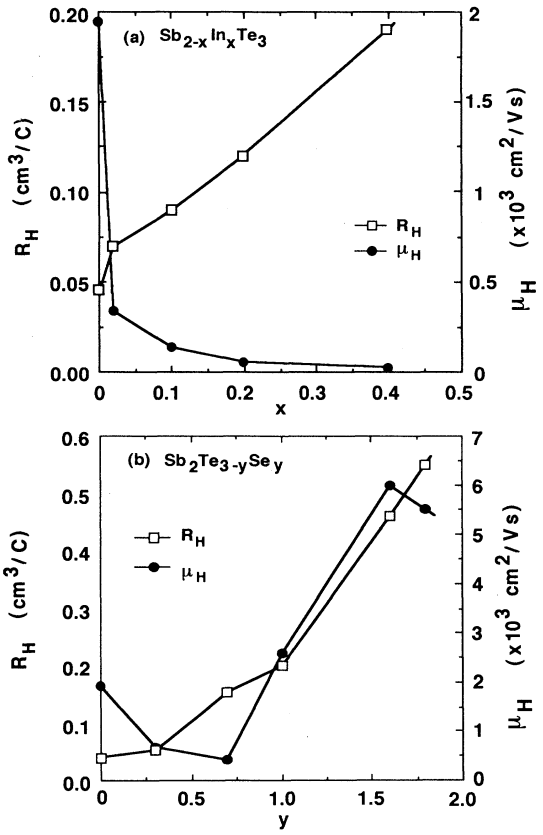

FIG. 2. Hall coefficients R_H and Hall mobilities μ_H at 4.2 K plotted against (a) In content x for $Sb_{2-x}In_xTe_3$ and (b) Se content y for $Sb_2Te_{3-y}Se_y$.

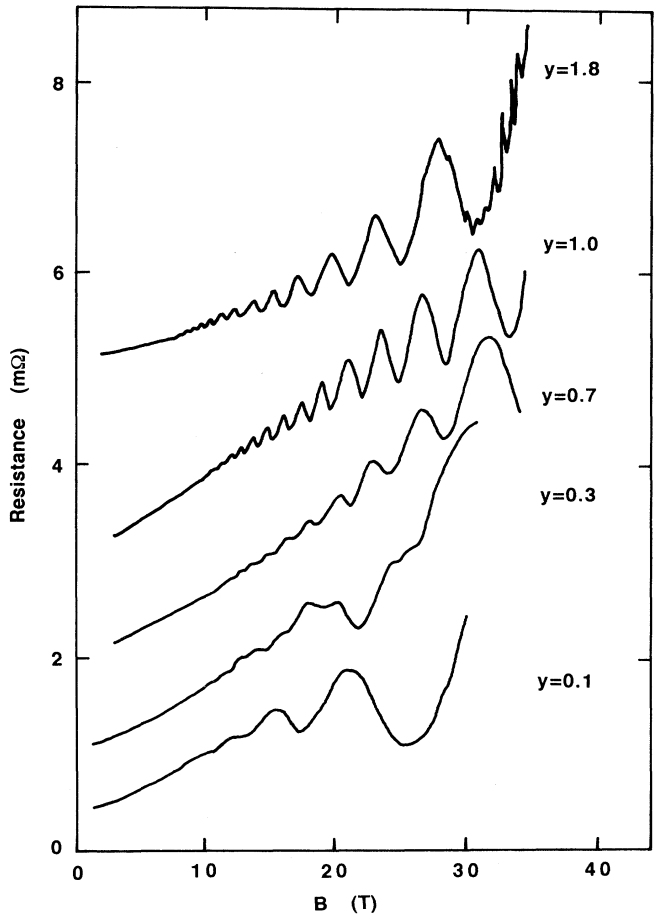

FIG. 4. SdH oscillations under the magnetic field B, parallel to the C_3 axis for $Sb_2Te_{3-y}Se_y$ ($y = 0.1$, 0.3, 0.7, 1.0, and 1.8) at 4.2 K.

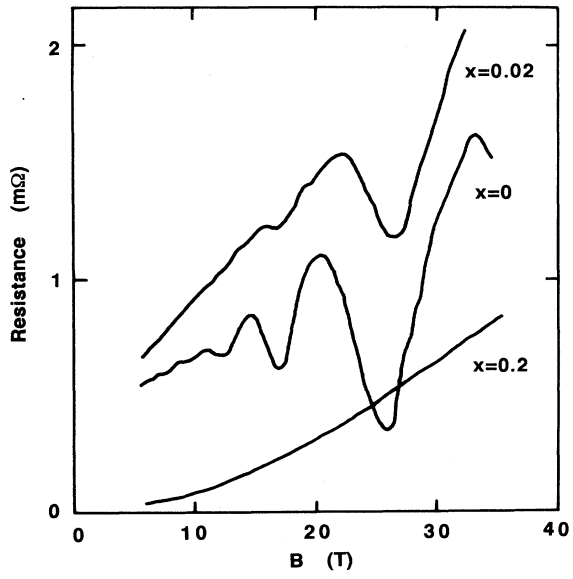

FIG. 3. SdH oscillations under the magnetic field B, parallel to the C_3 axis for $Sb_{2-x}In_xTe_3$ ($x = 0$, 0.02, and 0.2) at 4.2 K.

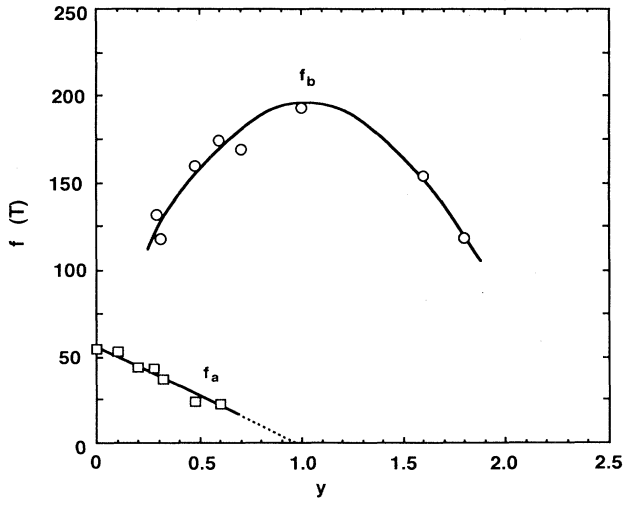

FIG. 5. SdH oscillation frequencies f_a and f_b at 4.2 K plotted against Se content y for $Sb_2Te_{3-y}Se_y$.

$y > 0.2$, indicating the presence of a different frequency. The Fourier transforms of the SdH oscillations give us the frequency components, which are plotted against Se concentration y in Fig. 5. The main frequency f_a, which corresponds to the extremal cross section of the Fermi surfaces of the UVB of Sb_2Te_3, falls with increasing y (which indicates that the cross-sectional area of the UVB is decreased with the Se content), and disappears near $y = 1.0$ according to the extrapolation. A frequency component f_b appears for samples with $y > 0.2$, which increases up to $y = 1.0$, followed by a decrease. This frequency can be ascribable to a valence band (thereafter denoted by NVB), as it will be discussed later. In addition, we have found a much higher-frequency component $f_c = 1600$ T for sample with $y = 1.8$. Using these data, together with the following TTE data, we shall discuss the possible band model for these solid solutions.

B. Transient thermoelectric effect

Figure 6 shows typical photoinduced TTE signals along the C_2 direction for $Sb_{2-x}In_xTe_3$ ($x = 0$ and 0.2) and $Sb_2Te_{3-y}Se_y$ ($y = 0.2$, 0.5, and 1.0) at $T = 300$ K in the time intervals 0–20 μs, where the observed TTE signals are averaged out by 15–20 times, because of extremely small magnitudes compared to those of the similar family of $Bi_{2-x}Sn_xTe_3$ crystals.[14] For the host material Sb_2Te_3, immediately after the laser irradiation, the induced TTE voltage $V(t)$ decreases drastically within 50 ns (minimum sampling time) and increases with time t up to about 25 μV in the short-time range 0–20 μs. Similar TTE profiles are also observed for the solid solutions.

As in the case for various solids,[10–14] the TTE voltages $V(t)$ at time t can be expressed in the exponential form,

$$V(t) = V_0 + \Sigma a_i \exp(-t/\tau_i) , \quad (1)$$

where V_0 is a constant value at $t \to \infty$, a_i a relaxation amplitude, and τ_i a relaxation time for the ith relaxation process or the type of carriers; $a_i > 0$ or $a_i < 0$ corresponds to a thermal diffusion of electrons or holes, respectively. From the analyses of the observed TTE signals, we have obtained four kinds of relaxation times τ_i ($i = 1-4$), due to "holes" ($a_i < 0$) for the host material and for In-substituted samples ($x \leq 0.2$). For Se-substituted ones, we have also four relaxation times $\tau_1 - \tau_4$, but the TTE signal corresponding to τ_1 becomes too weak for higher Se concentration $y > 1.0$. Moreover, two extra relaxation times τ_i ($i = 5$ and 6; $a_i < 0$) are observed for a higher Se concentration $y \geq 0.7$. Figures 7(a) and 7(b) plot the values of τ_i for $Sb_{2-x}In_xTe_3$ and

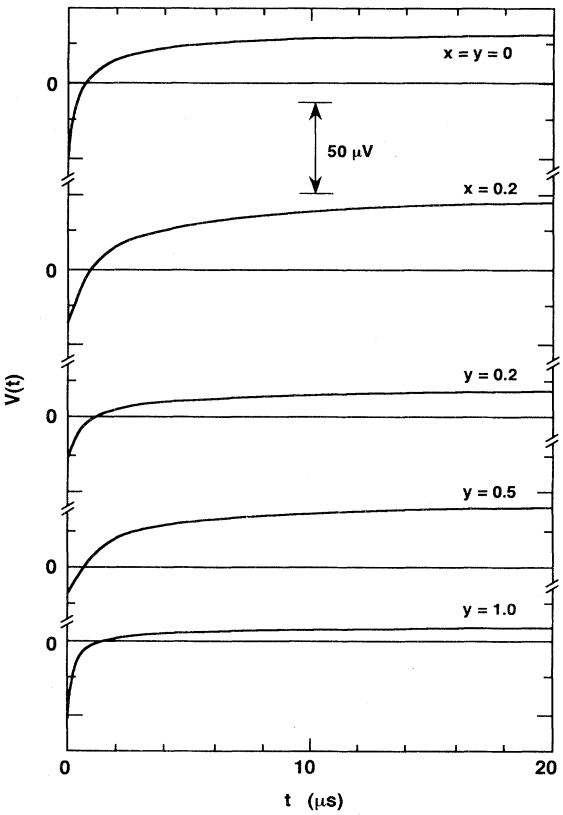

FIG. 6. Typical photoinduced TTE voltages $V(t)$ for $Sb_{2-x}In_xTe_3$ ($x = 0$, 0.2) and $Sb_2Te_{3-y}Se_y$ ($y = 0.2$, 0.5, and 1.0) along the C_2 axis at 300 K.

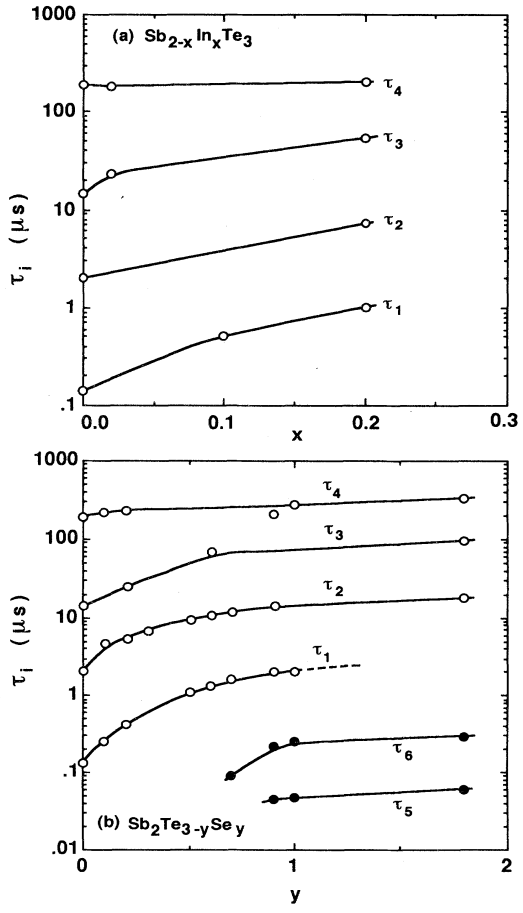

FIG. 7. (a) Observed relaxation times τ_i ($i = 1-4$) for $Sb_{2-x}In_xTe_3$ ($0 \leq x \leq 0.2$) plotted against In content x and (b) those of τ_i ($i = 1-6$) for $Sb_2Te_{3-y}Se_y$ ($0 \leq y \leq 1.8$) plotted against Se content y.

$Sb_2Te_{3-y}Se_y$ against x and y in semilogarithmic scales, respectively, where we see that these values span a wide time range from 10^{-2} to 10^2 μs, and that all relaxation times increase with x or y.

IV. DISCUSSIONS

A. $Sb_{2-x}In_xTe_3$

It is known that the UVB of the host Sb_2Te_3 consists of six equivalent valleys, similar to that of the same family of Bi_2Te_3, whose Fermi surfaces have an ellipsoidal shape tilted by about 50° from the C_1C_2 basal plane (perpendicular to the C_3 direction),[1,2] as shown schematically in Fig. 8(Ia), where the top view of the schematic Fermi surfaces of the UVB in the C_1C_2 plane is illustrated in the Brillouin zone. In fact, our observed SdH oscillation for Sb_2Te_3 shows only the single frequency component f_a, indicating that all the Fermi surfaces are equivalent in the C_3 direction. In addition, arrows mark the two valleys with different effective masses along the C_2 direction, to which we attribute the observed relaxation times τ_1 and τ_2 of the TTE signals, as indicated. On the other hand, much less is known about the Fermi surface of the LVB. In order to explain our experimental results reasonably, we propose a six-valley model for the LVB, as in the case for Bi_2Te_3,[14] where we assign another two relaxation times τ_3 and τ_4 to two different valleys of the LVB along the C_2 direction, similar to the case of the UVB [Fig. 8(Ia)]; however, its location in the Brillouin zone is unknown. The schematic band structure of Sb_2Te_3 is shown in Fig. 8(Ib), with which we shall give discussions about transport parameters (see later).

Now according to the ellipsoidal nonparabolic model,[2,3] the energy spectrum of the holes in the UVB of Sb_2Te_3 is represented in the form

$$2m_0E=h^2(\alpha_{11}k_1^2+\alpha_{22}k_2^2+\alpha_{33}k_3^2+2\alpha_{23}k_2k_3)\ , \tag{2}$$

where the inverse mass tensor components α_{ij} depend on the energy. Here, the momentum k_1, k_2, and k_3 form the Cartesian coordinates, which are parallel to one of the binary and bisectrix axes, and to the trigonal axis, respectively. The period of SdH oscillations $\Delta(1/B)$ in this model is connected with these parameters, as

$$\Delta\left[\frac{1}{B}\right]=\frac{eh}{m_0E_F}[(\alpha_{22}\alpha_{33}-\alpha_{23}^2)\cos^2\alpha+\alpha_{11}\alpha_{33}\cos^2\beta+\alpha_{11}\alpha_{22}\cos^2\gamma+2\alpha_{11}\alpha_{23}\cos\beta\cos\gamma]^{1/2}\ . \tag{3}$$

Here, $\cos\alpha$, $\cos\beta$, and $\cos\gamma$ are the direction cosines of the magnetic field B relative to the k_i axis ($i=1,2,3$) in the momentum space, respectively. We have calculated the hole concentrations p_{SdH} at 4.2 K, for $Sb_{2-x}In_xTe_3$, using the parameters of the energy spectrum for Sb_2Te_3,[2] where we have assumed that the anisotropy of the Fermi surface and tilt angle of the ellipsoids do not depend on the In concentration. These values, together with those evaluated from the Hall effect p_H, are compared in Table I. We note that with increasing In content the hole concentration is decreased, which may due to the suppression of antistructural defects formed in the host material. In addition, p_H is larger than p_{SdH} in each sample, which means that the holes in the UVB with p_{SdH} are responsible for the SdH effect, while those in the LVB are not, due to very low mobility; thus, p_{SdH} is regarded as the hole concentration p_U in the UVB.

On the other hand, the theoretical analysis of the diffusion equation for photogenerated carriers gives the following relation between the relaxation time τ_i and carrier mobility μ_i of the ith carrier:[10]

$$\tau_i=eL_i^2/(2k_BT\mu_i)\ \text{ or }\ \mu_i=eL_i^2/(2k_BT\tau_i)\ , \tag{4}$$

where L_i is a diffusion length, which, we assume, is independent of the type of carriers ($L_i=L$).[10–14] Based on the above two-valence-band model, we have evaluated the hole concentration p_U in the UVB, p_L in the LVB, and their mobility μ_i along the C_2 axis corresponding to τ_i

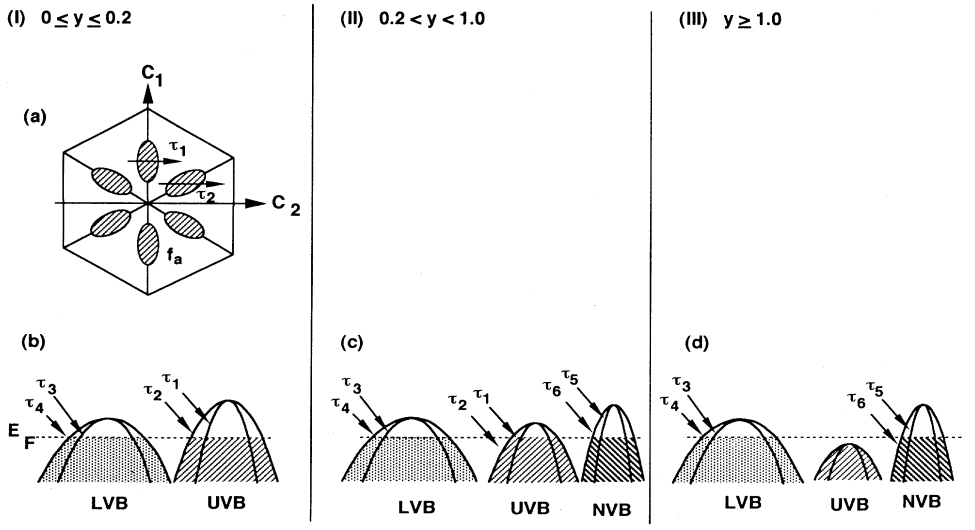

FIG. 8. Schematic valence-band model for $Sb_2Te_{3-y}Se_y$ in different Se concentration regions; (I) $y\le0.2$, (II) $0.2<y<1.0$, and (III) $y\ge1.0$ (see text).

TABLE I. Hole concentration p_H evaluated from the Hall coefficient, p_{SdH} from the SdH effect (which is assumed to be equal to the hole concentration p_U in the UVB), p_L in the LVB, parameters α and β, hole mobilities μ_1 and μ_3, and effective-mass ratios m_2^*/m_1^* and m_4^*/m_3^* evaluated using the two-valence-band model for $Sb_{2-x}In_xTe_3$ ($x \leq 0.2$) (see text).

x	p_H	$p_{SdH}=p_U$ (10^{20} cm^{-3})	p_L	α (10^{-2})	β (10^2)	μ_1 (cm^2/V s)	μ_3	m_2^*/m_1^*	m_4^*/m_3^*
0	1.55	0.23	90	0.93	3.9	8000	81	2.9	2.8
0.02	0.89	0.20	80	0.78	4.0	1400	11		2.3
0.1	0.69	0.18	41	1.3	2.3	560	7.3		
0.2	0.52							2.2	1.7

using Eq. (4), as in the following way. Here, it is to be noted that to the carrier transport along the C_2 direction, there contribute two equivalent hole pockets corresponding to τ_1 (or carrier mobility μ_1) and four corresponding to τ_2 (or μ_2) in the UVB, as shown in Fig. 8(Ia). Similarly, for the LVB we propose two equivalent pockets corresponding to τ_3 (or μ_3) and four ones with τ_4 (or μ_4). Also, we have taken account of the inequalities for these quantities; $\tau_1 \ll \tau_2$ (or $\mu_1 \gg \mu_2$) and $\tau_3 \ll \tau_4$ (or $\mu_3 \gg \mu_4$).

Thus, the total conductivity σ, Hall coefficient R_H, and Hall mobility μ_H can be written as

$$\sigma = e\{(\tfrac{2}{6})p_U\mu_1 + (\tfrac{4}{6})p_U\mu_2 + (\tfrac{2}{6})p_L\mu_3 + (\tfrac{4}{6})p_L\mu_4\}$$
$$\cong (e/3)(p_U\mu_1 + p_L\mu_3) = (e/3)p_U\mu_1(1+\alpha\beta) , \quad (5)$$

$$R_H = (1/e)\{(\tfrac{2}{6})p_U\mu_1^2 + (\tfrac{4}{6})p_U\mu_2^2 + (\tfrac{2}{6})p_L\mu_3^2 + (\tfrac{4}{6})p_L\mu_4^2)\}$$
$$\times\{(\tfrac{2}{6})p_U\mu_1 + (\tfrac{4}{6})p_U\mu_2 + (\tfrac{2}{6})p_L\mu_3 + (\tfrac{4}{6})p_L\mu_4\}^{-2}$$
$$\cong (3/ep_U)(1+\alpha^2\beta)/(1+\alpha\beta)^2 , \quad (6)$$

$$\mu_H \cong \mu_1(1+\alpha^2\beta)/(1+\alpha\beta) , \quad (7)$$

with $\alpha = \mu_3/\mu_1$ ($=\tau_1/\tau_3$) and $\beta = p_L/p_U$ (electron charge $e>0$). Taking into account the experimental fact that R_H is almost independent of temperature, we assume that the parameters α and β in Eqs. (5)–(7) are also temperature independent. According to Eq. (4), the mobility ratio α is expressed by the ratio for the relaxation times of the UVB and LVB, τ_1 and τ_3, respectively, measured along the C_2 axis [Fig. 7(a)]. The hole concentration p_U in the UVB is regarded as equal to the observed value p_{SdH} from the SdH effect, using Eq. (3) with parameters that were determined for Sb_2Te_3.[2] The total hole concentration $p_H = 1/eR_H$ was calculated from the observed Hall coefficient [Fig. 2(a)]. With the values of p_U and α, we get the parameter β using Eq. (6), from which we obtain the hole concentration p_L in the LVB. The observed Hall mobility μ_H is further approximated by $\mu_H = \mu_1/(1+\alpha\beta)$ (since $\alpha^2\beta \ll 1$) in Eq. (7), with which we obtain the value of μ_1 and thus the carrier mobility μ_3 for the LVB from α. These evaluated parameters are complied in Table I. The hole concentrations p_U and p_L are decreased with increasing In content, primarily due to the suppression of the antistructural defects by incorporating of In atoms into the Sb lattices. We should also note that the hole mobility μ_1 of the UVB is much larger than μ_3 of the LVB, and these values are drastically reduced with x, which indicates that ionized or neutral impurity scatterings by these crystal defects become predominant.

Moreover, the substitution of In atoms into Sb sites in Sb_2Te_3 may affect the anisotropy of the ellipsoidal Fermi surfaces of the UVB and LVB. To estimate the anisotropy in the effective mass, we use the following relation:

$$\tau_j/\tau_i = \mu_i/\mu_j = (m_j^*/m_i^*)^\gamma , \quad (8)$$

where γ is a parameter characterizing a scattering mechanism. Assuming phonon scatterings for all carriers in each pocket ($\gamma = \frac{5}{2}$), from Eq. (8) with the observed relaxation times at 300 K [Fig. 7(a)], we obtain the effective mass ratio with respect to m_1^* for the UVB, m_2^*/m_1^*, and that for the LVB with respect to m_3^*, m_4^*/m_3^*, as listed in Table I. We see that the anisotropy in the effective mass of the UVB is of the same order of magnitude as that of the LVB for the host material (about 3), and these values decrease with In alloying. In particular, the reduction is appreciable for the latter, which may arise from the increasing in the tilt angle θ with In alloying.

B. $Sb_2Te_{3-y}Se_y$

To our knowledge, there is no available information about the band parameters in Eq. (2) for the solid solution of $Sb_2Te_{3-y}Se_y$. Hence, in the present work, based on our band model (Fig. 8), we have attempted to evaluate the hole concentrations p_U and p_L, and hole mobilities μ_1, μ_3, and μ_5 of the UVB, LVB, and valence band, respectively, using the observed Hall data [Fig. 2(b)], the SdH frequencies f_a and f_b (Fig. 5), and TTE data τ_i [Fig. 7(b)]. We should note that there are three different regions of Se concentration: In the first region $0 \leq y \leq 0.2$, there is only one frequency component in the SdH effect, but the Hall concentration is higher than the SdH concentration, and we have observed four relaxation times. In the second region $0.2 < y < 1.0$, there are two frequency components f_a and f_b, and two additional relaxation times τ_5 and τ_6 are detected for $y \geq 0.7$, which we have attributed to a different valence band, with an anisotropic and small effective mass, as discussed later. The frequency f_b increases with y up to $y = 1.0$ and then decreases (Fig. 5). The increase in the frequency with y in the range $0.2 < y < 1.0$ is due to the change of the positions of the UVB, LVB, and valence band; the valence band moves up and UVB moves down, due to Se doping [(Fig. 8(c)]. For $y \geq 1.0$, there are two extremes filled by holes, valence band and LVB, because UVB disappears according to the

extrapolation (Fig. 5).

In view of these, we propose the most likely band structure for the solid solutions with three regions, $0 \le y \le 0.2$, $0.2 < y < 1.0$, and $1.0 \le y \le 1.8$, as depicted schematically in Figs. 8(I), 8(II), and 8(III), respectively. The Fermi surfaces in the C_1C_2 plane for the UVB consist of two types of hole valleys with the relaxation times τ_1 and τ_2, as marked by arrows in Fig. 8(Ia). We assume that the LVB is the same as that of the host [Fig. 8(Ia)], that has a multivalley structure consisting of two types of hole valleys with the relaxation times τ_3 and τ_4 in the whole region of Se concentration.

With this model, we have evaluated the carrier concentration p_U, for the UVB in the region I from the observed SdH frequency f_a, using Eq. (3) with the parameters that are extrapolated from those for Sb_2Te_3.[2] Then using Eqs. (5)–(8) with the experimental values of α and Hall-effect data, the values of β can be evaluated according to the procedure similar to that for $Sb_{2-x}In_xTe_3$. All calculated values are listed in Table II. We note that the carrier mobilities are decreased with y drastically, which may be due to an appreciable increase of ionized and/or neutral scattering centers by substituting Se atoms into Te lattices.

However, this procedure is not acceptable for $0.2 < y < 1.0$, because in this region II, we have simultaneously three valence bands, UVB, LVB, and valence band [Fig. 8(II)], where the valence band is supposed to consist of six ellipsoids with a small anisotropy compared to that of the UVB. With such a three-valence-band model, the Hall coefficient R_H and the Hall mobility μ_H are written as

$$R_H = (3/ep_U)(1+\alpha^2\beta+\delta^2\varepsilon+2\gamma^2\varepsilon)/(1+\alpha\beta+\delta\varepsilon+2\gamma\varepsilon)^2 , \quad (9)$$

$$\mu_H = \mu_1(1+\alpha^2\beta+\delta^2\varepsilon+2\gamma^2\varepsilon)/(1+\alpha\beta+\delta\varepsilon+2\gamma\varepsilon) , \quad (10)$$

respectively, where $\alpha=\mu_3/\mu_1$, $\beta=p_L/p_U$, $\gamma=\mu_6/\mu_1$, $\delta=\mu_5/\mu_1$, and $\varepsilon=p_N/p_U$ (p_U is the hole concentration in the valence band). Here, we note that $\mu_1 \gg \mu_3 (\tau_1 \ll \tau_3)$, $\mu_3 \gg \mu_4$ ($\tau_3 \ll \tau_4$), and $\mu_5 \sim 5\mu_6$ [$\tau_5 \sim (\frac{1}{5})\tau_6$; see Fig. 7(b)]; thus, in actual the terms, $2\gamma^2\varepsilon$ in the above expressions is negligibly small.

For the self-consistent fitting in this region II using Eqs. (2), (3), (9), and (10), we need simultaneously the static transport, SdH effect, and dynamic TTE data. The parameter α can be readily obtainable from the observed relaxation times τ_1 and τ_3, while δ cannot be obtained because τ_5 is unknown in this region; we then extrapolate the data at the value at $y=0.7$ ($\tau_5=0.035$ μs) from Fig. 7(b) to get the parameter δ for $y=0.7$ ($\delta=45$). Since the parameter β in the region I is seen to be nearly constant [$(2.1-3.7)\times10^2$], we use the averaged value of $\beta=2.7\times10^2$ for the region II. On the other hand, the hole concentrations p_U are estimated from the values of f_a, using Eqs. (2) and (3) with the band parameters for $(Bi_{1-x}Sb_x)_2Te_3$ ($0<x<1$);[2] we obtain a good relationship between f_a and p_U, as $p_U \propto f_a^{3/2}$, which is used also for the valence band, as $p_N \propto f_b^{3/2}$ (see below). The value of f_a for $y=0.7$ is also evaluated to be 14 T from the extrapolation of the experimental data (Fig. 5). Thus, only for $y=0.7$, have we obtained the best-fit parameters ε, μ_1, p_N ($=\varepsilon p_U$), and μ_5 ($=\delta\mu_1$) for the valence band using Eqs. (9) and (10). To calculate p_N for other Se concentrations, furthermore, we have assumed that the anisotropy of the Fermi surfaces is constant in the region II, where we use the relation $p_N \propto f_b^{3/2}$. With the above procedure, Table II lists the available parameters in the region II.

Moreover, for the region III with $y \ge 1.0$, we have attempted to evaluate the parameters using the two-valence-band model and Eqs. (5)–(7), with the same approximation for the shape of the valence band as was done for $y=0.7$. Here, we define $\alpha'=\mu_3/\mu_5$ and $\beta'=p_L/p_N$. According to the procedure as done in the region I, we have evaluated these values, including the hole mobilities μ_3 and μ_5 at 300 K, as listed in Table II. We note that the carrier mobility of the valence band μ_5 in this region is particularly large. However, for $y=1.6$ and 1.8, it is difficult to fit all data under the assumption that the tilt angle and the shape of the ellipsoids of the

TABLE II. Best-fit parameters for $Sb_2Te_{3-y}Se_y$ in the Se concentration regions, (I) $0 \le y \le 0.2$, (II) $0.2 < y < 1.0$, and (III) $y \ge 1.0$ (see text).

Region	y	p_U	p_L (10^{19} cm^{-3})	p_N	α (10^{-2})	α' (10^{-4})	β (10^2)	β'	δ	ε	μ_1	μ_3 (cm^2/V s)	μ_5
	0	2.43	900		0.93		3.7				8210	76	
(I)	0.1	2.25	540		1.3		2.4				2630	34	
	0.2	1.70	360		1.6		2.1				1810	29	
	0.25	1.64		4.7	1.8		(2.7)			2.9			
	0.3	1.34		3.9			(2.7)			2.9			
(II)	0.5	0.73		6.3	1.8		(2.7)			8.6			
	0.6	0.60		7.1	1.8		(2.7)			12			
	0.7	0.30		6.6	2.3		(2.7)		45	22	12	0.3	540
	1.0		570	7.0		7.0		81				2.0	2750
(III)	1.6		120	4.0		7.2		29				5.7	7900
	1.8		140	3.2		7.5		43				5.5	7290

valence band are constant; if this is the case, we have to reduce p_N by 30%. Thus the anisotropy or tilt angle should change in the valence band ellipsoids by Se doping. Moreover, the ratio f_a/f_b from Fig. 5 is found to be approximately equal to $\beta^{2/3}$, from which we may ascribe the observed high frequency f_c (1,600 T) of the SdH effect for $y=1.8$ to the LVB. The hole concentrations p_U and p_L for $Sb_2Te_{3-y}Se_y$ are decreased with increasing y, indicating that the energy gap between the valence and conduction bands is increased, similar to that found for the $Sb_{2-x}In_xTe_3$ system.[7,8]

Finally, we have estimated an anisotropy in the effective-mass ratio m_i^*/m_j^* for each band, using Eq. (8) with the observed relaxation times for $Sb_2Te_{3-y}Se_y$ along the C_2 axis; $m_2^*/m_1^*=3-2$ for UVB and $m_4^*/m_3^*=3-1.5$ for LVB in the range $0\le y\le 1.8$, indicating that the anisotropies for these bands are decreased by substituting Se atoms into the host Sb_2Te_3, which may be due to the increase in the tilt angle of the ellipsoidal Fermi surface, with respect to the basal plane of each band, rather than the change in its size. On the other hand, the ratio m_6^*/m_5^* for the valence band in the range $0.9\le y\le 1.8$ is found to be almost constant ($\cong 2$). We also note that the effective-mass ratio for the valence band with respect to UVB, m_5^*/m_1^*, is obtained to be 0.2, which in turn means that the carrier mobility in the valence band is extremely large (see Table II). Theoretical band calculations for these solid solutions will be required to confirm the above model.

V. CONCLUSION

From the static and dynamic transport measurements for solid solutions of p-type $Sb_{2-x}In_xTe_3$ ($0\le x\le 0.4$) and $Sb_2Te_{3-y}Se_y$ ($0\le y\le 1.8$) along the C_2 axis, we have found the following features. There are systemic variations of the Hall coefficient and Hall mobility with In content x and Se content y below $y\le 0.2$. The most significant change in the band structure for $Sb_2Te_{3-y}Se_y$ is the appearance of the valence band above $y=0.2$, as found from the SdH effect and TTE experiments. The observed TTE voltages are characterized by a multiple relaxation process with a different relaxation time τ_i ($i=1-6$) for thermal diffusions of photogenerated carriers, where τ_1 and τ_2 are due to holes in the UVB, τ_3 and τ_4 to LVB, and τ_5 and τ_6 (observable only for $y\ge 0.7$) are due to the valence band with extremely large mobilities, which may originate from the valence bands of the constituent counterpart of Sb_2Se_3. Based on these experimental data, we have proposed the most probable band models for these solid solutions. The anisotropy in the effective mass in each band is evaluated, which indicates that the multivalley model is valid for the Sb_2Te_3 based solid solutions.

ACKNOWLEDGMENTS

One of the authors (V.A.K.) would like to thank the International Science Foundations (USA) for carrying out part of the work at Moscow State University, and the Japan Society for the Promotion of Science for financial support during his sabbatical stay at the Department of Materials Science, Hiroshima University. Part of the work was also supported by the Grants from the Chugoku-Denryoku Science Foundations, and Grant-In-Aid from the Ministry of Education and Culture, Japan.

[1] A. von Middendorf, K. Dietrich, and G. Landwehr, Solid State Commun. **13**, 443 (1973).
[2] H. Köhler and A. Freudenberger, Phys. Status Solidi B **195**, 195 (1977).
[3] J. R. Drabble and R. Wolf, Proc. R. Soc. London **69**, 1101 (1956).
[4] G. Simon and W. Eichler, Phys. Status Solidi B **107**, 207 (1981).
[5] J. Horak, K. Cermak, and L. Koudelka, J. Phys. Chem. Solids **47**, 805 (1986).
[6] J. Horak, P. Lostak, and L. Benes, Philos. Mag. B **50**, 665 (1984).
[7] P. Lostak, R. Novotny, J. Kroutil, and Z. Stary, Phys. Status Solidi A **104**, 841 (1987).
[8] J. Kroutil, J. Navratil, and P. Lostak, Phys. Status Solidi A **131**, k73 (1992).
[9] M. Storder, H. T. Langhammer, H. Sobota, and V. Riede, Phys. Status Solidi B **104**, 513 (1981).
[10] M. Sasaki, H. Negishi, and M. Inoue, J. Appl. Phys. **59**, 796 (1986).
[11] M. Sasaki, S. Horisaka, and M. Inoue, Jpn. J. Appl. Phys. **26**, 1704 (1987).
[12] M. Sasaki, G. X. Tai, S. Tamura, and M. Inoue, Phys. Rev. B **47**, 6216 (1993).
[13] M. Sasaki, G. X. Tai, M. Inoue, and H. Bidadi, J. Appl. Phys. **75**, 4520 (1994).
[14] V. A. Kulbachinskii, M. Inoue, M. Sasaki, H. Negishi, W. X. Gao, K. Takase, Y. Giman, P. Lostak, and J. Horak, Phys. Rev. B **50**, 16 921 (1994).
[15] V. M. Koshkin, L. P. Gal'chinetskii, V. N. Kulik, B. I. Minkov, and U. A. Ulmanis, Solid State Commun. **13**, 1 (1973).
[16] G. Micocci, A. Tepore, R. Rella, and P. Siciliano, Phys. Status Solidi B **126**, 437 (1991).